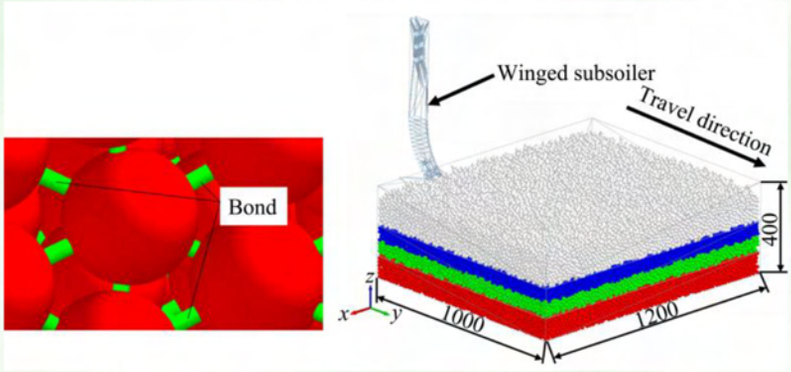

a. Cylindrical bonds between particles b. Discrete element model developed by EDEM

Figure 5 Cylindrical bonds between particles and the discrete element model developed using EDEM

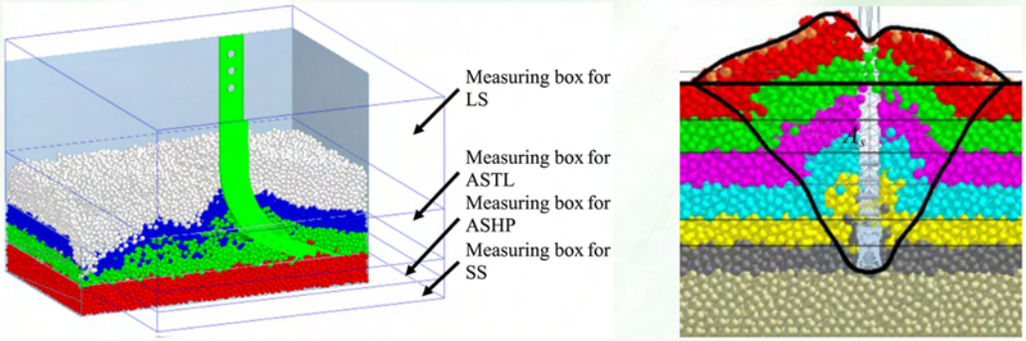

a. Measuring tillage forces of different sections of subsoiler b. Furrow profile and area A_s

Figure 6 Measurement of tillage forces of subsoiler and soil disturbance area

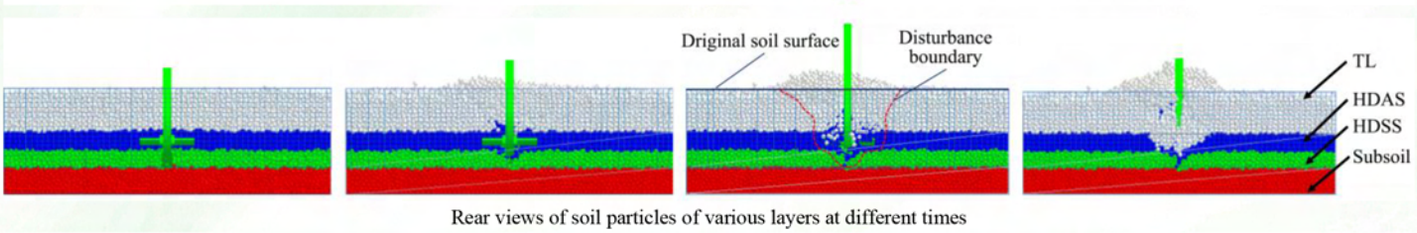

Rear views of soil particles of various layers at different times

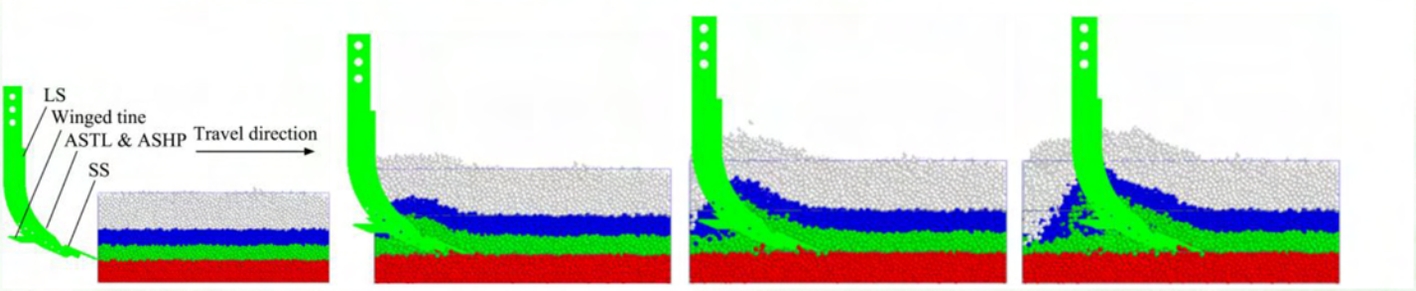

Side views of soil particles of various layers at different times

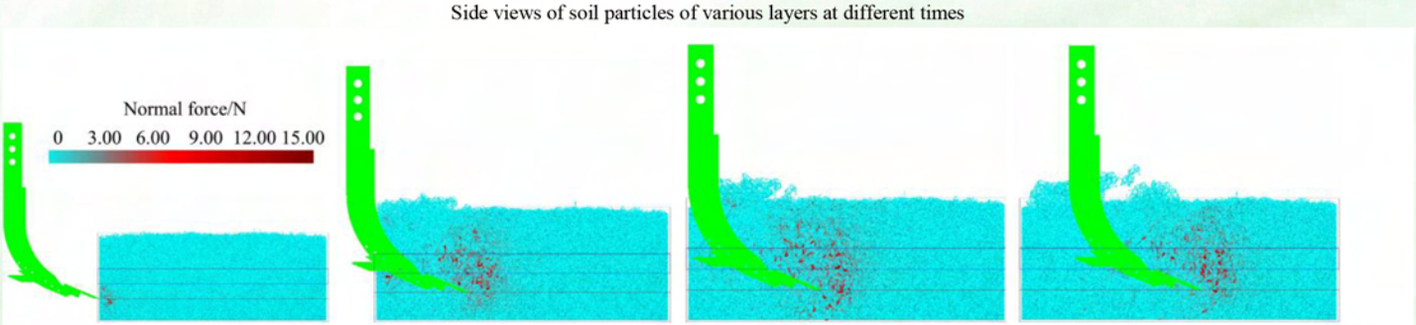

Side views of bonds between soil particles at different times

a. 5.28 s b. 5.66 s c. 5.78 s d. 5.96 s

Figure 9 Soil disturbance behaviors at different times under the action of the winged subsoiler

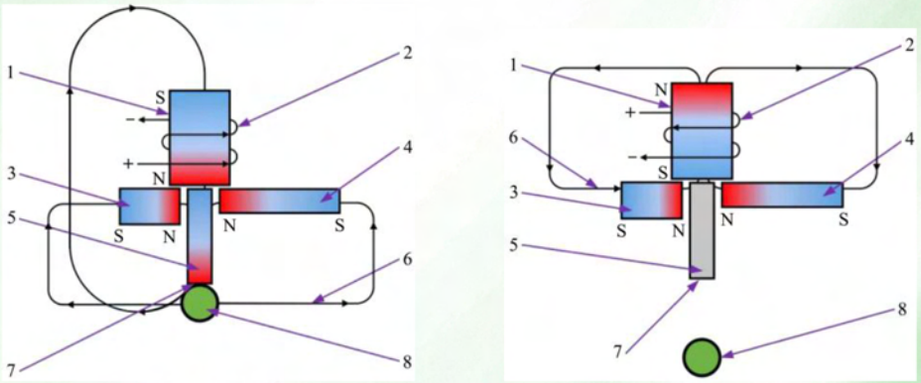

a. Attractive state b. Clearing state

1. Iron core 2 Coil 3. Permanent-magnet I 4. Permanent-magnet II 5. Magnetic head 6. Magnetic induction line 7. Seeding plane 8. Pelleted seed.

Figure 1 Structure of CMS component and magnetic-circuit directions in two working states

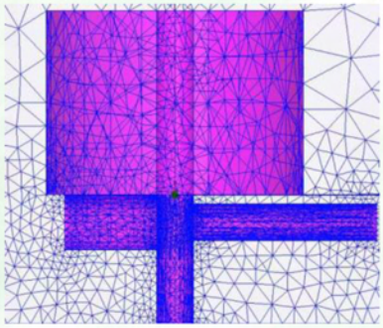

Figure 2 Computational grids of the CMS component

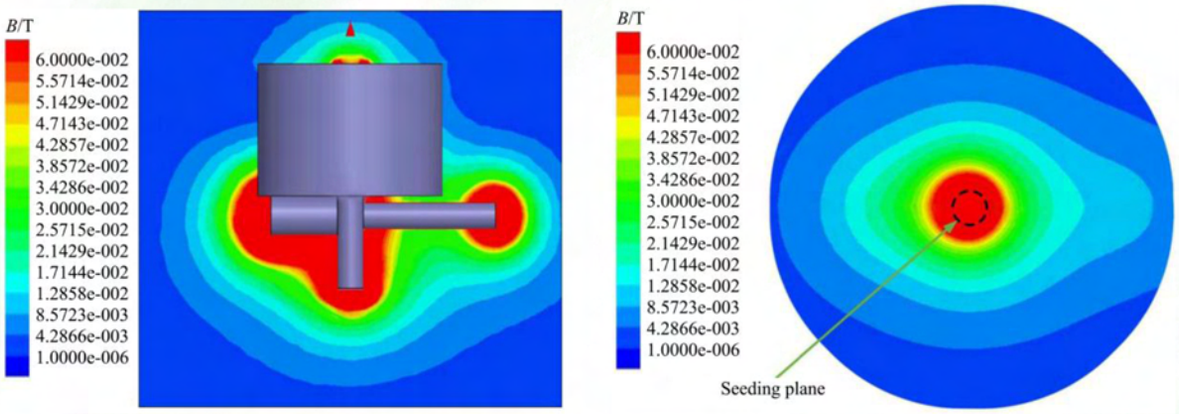

a. Around the CMS component b. On the seeding plane

Figure 4 Magnetic flux density distribution of the CMS component working in the attractive state

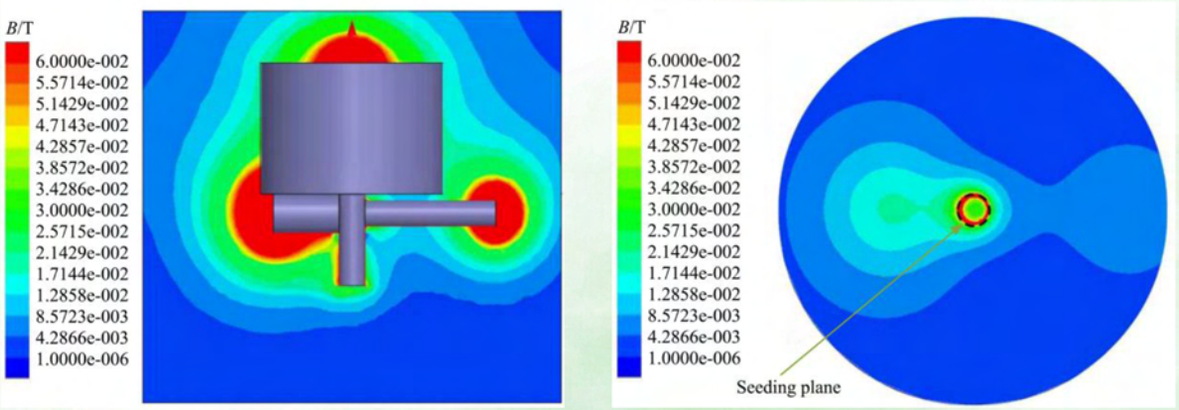

a. Around the CMS component b. On the seeding plane

Figure 5 Magnetic flux density distribution when the CMS component works in the clearing state